

Substrate-Assisted Catalysis in the Reaction Catalyzed by Salicylic Acid Binding Protein 2 (SABP2), a Potential Mechanism of Substrate Discrimination for Some Promiscuous Enzymes

Jianzhuang Yao,^{†,‡} Haobo Guo,^{†,‡} Minta Chaiprasongsuk,[§] Nan Zhao,[§] Feng Chen,[§] Xiaohan Yang,^{||} and Hong Guo^{*,†,‡}

[†]Department of Biochemistry and Cellular and Molecular Biology, University of Tennessee, Knoxville, Tennessee 37996, United States

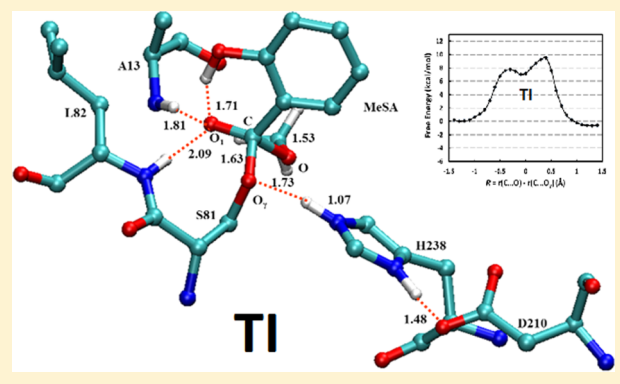
[‡]UT/ORNL Center for Molecular Biophysics, Oak Ridge National Laboratory, Oak Ridge, Tennessee 37830, United States

[§]Department of Plant Sciences, University of Tennessee, Knoxville, Tennessee 37996, United States

^{||}Biosciences Division, Oak Ridge National Laboratory, Oak Ridge, Tennessee 37831, United States

Supporting Information

ABSTRACT: Although one of an enzyme's hallmarks is the high specificity for their natural substrates, substrate promiscuity has been reported more frequently. It is known that promiscuous enzymes generally show different catalytic efficiencies to different substrates, but our understanding of the origin of such differences is still lacking. Here we report the results of quantum mechanical/molecular mechanical simulations and an experimental study of salicylic acid binding protein 2 (SABP2). SABP2 has promiscuous esterase activity toward a series of substrates but shows a high activity toward its natural substrate, methyl salicylate (MeSA). Our results demonstrate that this enzyme may use substrate-assisted catalysis involving the hydroxyl group from MeSA to enhance the activity and achieve substrate discrimination.



Enzymes are often considered to have been evolved to specifically catalyze the reactions involving their natural substrates, but the catalytic promiscuity of enzymes is not a new concept^{1,2} and has been reported frequently.^{3–6} The mechanism of promiscuity has been discussed recently in several reviews.^{7–11} Promiscuous enzymes generally show different catalytic efficiencies for different substrates.^{12,13} Although the possible factors that may lead to different catalytic efficiencies for different substrates have been discussed,¹⁰ there are still considerable uncertainties and a lack of detailed analyses concerning the exact energetic contributions from these factors. This is probably due in part to the complexity of the catalytic processes that make it difficult to clearly separate one interaction or factor from another. Here we focus on the analysis of the possible role and energetic contribution of substrate-assisted catalysis (SAC) for the reaction catalyzed by salicylic acid binding protein 2 (SABP2) through a combination of computational and experimental investigations. SAC is a process in which the functional groups from substrates, in addition to those from enzymes, contribute to the rate acceleration of the enzyme-catalyzed reactions.^{14–16} The removal of such functional groups is known to impair the catalysis. It has been demonstrated on some engineered enzymes that SAC may provide a way of drastically changing substrate specificity. Understanding the relationship between substrate promiscuity and SAC is of considerable importance for enzymology; it might be helpful for

protein engineering^{17,18} and drug design,^{19,20} as well. Nevertheless, a detailed analysis concerning how naturally occurring enzymes might have used SAC as one of the important strategies for discrimination between their natural substrates containing the SAC participating groups and other substrates that lack such groups is still lacking.

SABP2 belongs to the α/β fold carboxylesterase hydrolase superfamily (EC 3.1.1).^{21–25} Previous studies have demonstrated that SABP2 possesses specific esterase activity toward MeSA.²³ MeSA is a compound found in plants that can be produced from salicylic acid (SA) by the methylation activity of the SA methyltransferase (SAMT).²⁶ The conversion of MeSA back to salicylic acid (SA) catalyzed by SABP2 is believed to be a part of the signal transduction pathways that activate systemic acquired resistance and local defense responses to plant pathogens.^{21–25} It has been shown²¹ that Ser-81, His-238, and Asp-210 act as the catalytic triad (Figure 1), and the esterase activity was mostly or totally abrogated by the Ser81Ala mutation.²¹ The SABP2-catalyzed reaction consists of acylation and deacylation processes, and Figure 1 shows the proposed mechanism for the acylation reaction in which Ser-81 serves as

Received: June 10, 2015

Revised: July 25, 2015



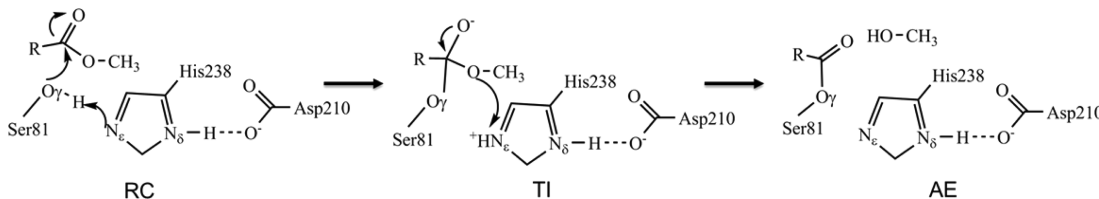


Figure 1. Acylation reaction mechanism in SABP2 with the catalytic triad involving Ser-81, His-238, and Asp-210. RC represents the reactant complex, TI the tetrahedral intermediate, and AE the acyl-enzyme complex. SABP2 can catalyze reactions for a number of substrates, including methyl salicylate (MeSA),^{21,25} methyl jasmonate (MeJA),^{21,25} methyl indole-3-acetic acid ester (MeIAA),^{21,25} acibenzolar-S-methyl,²⁸ 4-methylumbelliferonate butyrate,²³ *p*-nitrophenyl (pNP) palmitate, pNP myristate, pNP butyrate,²³ and pNP acetate.²⁷ Here we demonstrate that methyl benzoate (MeBA) is also a substrate of SABP2, and the increase in catalytic efficiency upon going from MeBA to MeSA is likely due to the participation of substrate-assisted catalysis.

the nucleophile and attacks the carbon atom of the ester bond. His-238, with help of Asp-210, functions as the general acid and base catalyst during the catalysis. It has been shown previously and in this work (Figure 1) that SABP2 can catalyze the reactions for a series of substrates,^{21–25,27,28} even though its activity on MeSA is much higher.^{21,25,27} One possible explanation is that the active site of SABP2 would be too crowded to be occupied by some relatively large substrates, leading to a decrease in activity,²¹ but other factors may also be involved.

The crystal structure of tobacco SABP2 complexed with salicylic acid (SA)²¹ reveals that the backbone amide group of Ala-13 in the enzyme participates in the oxyanion hole interaction through the hydrogen bonding interaction with the SA carbonyl oxygen atom, as shown in Figure 2. Another potential

MeSA to increase its activity and achieve substrate discrimination. The simplicity of the reaction catalyzed by SABP2 with relatively small substrates makes it possible to perform combined computational and experimental investigations and examine the role of SAC in detail during the catalysis.

To elucidate the role of the oxyanion–hole interaction involving the substrate in substrate promiscuity and discrimination, we have studied the SABP2-catalyzed reactions with MeSA and methyl benzoate (MeBA) as the substrates using free energy (potential of mean force) simulations (with the SCC-DFTB/MM Hamiltonian²⁹). An experimental study was also performed to confirm the theoretical prediction. The results from the combination of computational and experimental investigations suggest that the substrate-assisted three-pronged oxyanion hole involving MeSA may contribute to a higher catalytic efficiency and result in substrate discrimination between natural and some other promiscuous substrates.

EXPERIMENTAL PROCEDURES

Models. The initial coordinates for the reactant complexes were based on the crystallographic structure (Protein Data Bank entry 1Y7I, 2.1 Å resolution) of tobacco SABP2 in complex with SA.²¹ A methyl group was manually added to SA to form MeSA. The side chain of Ser-81 was manually placed between His-238 and the carbonyl carbon of MeSA to complete the catalytic triad (see above). Hydrogen atoms of protein were added by the HBUILD module³⁰ implemented in CHARMM,^{31,32} but the substrate hydrogen atoms were added manually. All ionizable residues were set to the standard protonated or deprotonated states under physiological conditions. A careful check of the surrounding environment of all histidine residues allowed the proton to be assigned to the N_ε or N_δ atoms for His residues. All protonation states were further confirmed with MOE.³³ The reactant complex was solvated by water droplets with a 22 Å radius by the standard superimposing protocol with the center located at the Ser-81 oxygen atom (O_y labeled in Figure 2), and solvent water molecules within 2.8 Å of any crystal atoms were removed. A modified TIP3P water model^{34,35} was employed for the solvent. The substrates and the side chains of Ser-81, His-238, and Asp-210 were treated by QM, and the rest of the system was treated by MM. The link-atom approach³⁶ implemented in CHARMM³² was applied to separate the QM and MM regions. The DIV scheme³⁷ implemented in CHARMM was used to treat the QM/MM frontier. The SCC-DFTB method³⁸ with empirical dispersion corrections³⁹ implemented in CHARMM was used for the QM atoms, and the all-hydrogen CHARMM potential function (PARAM27)⁴⁰ was used for the MM atoms. For the reactant complex containing MeBA, the hydroxyl group

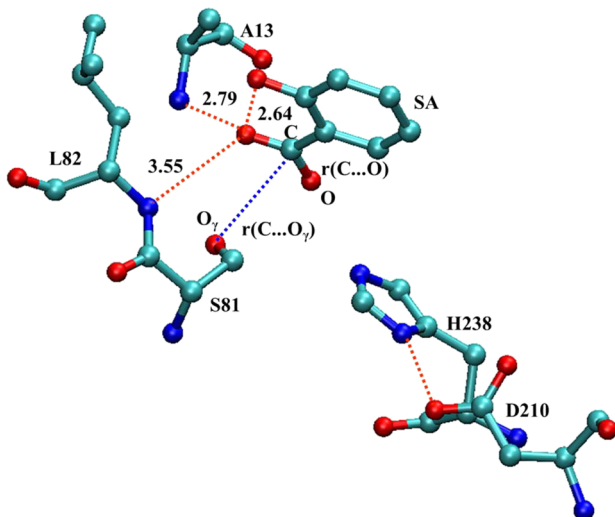


Figure 2. Active site of SABP2 from the X-ray crystal structure (Protein Data Bank entry 1Y7I) obtained in ref 21. The Reaction coordinate is $RC = r(C\cdots O) - r(C\cdots O_y)$. All distances are in angstroms.

hydrogen bond involved in oxyanion hole stabilization is from the backbone amide group of Leu-82. However, this hydrogen bond seems rather weak, as demonstrated by the fact that the corresponding hydrogen-bond distance is 3.55 Å in the product complex (between the non-hydrogen atoms). The third hydrogen-bond donor for the oxyanion hole interaction is the hydroxyl group from the substrate; the corresponding hydrogen-bond distance is 2.66 Å between the two oxygen atoms (Figure 2). An interesting question is whether SABP2 may use the SAC mechanism through the enhancement of the oxyanion–hole interaction involving this hydroxyl group

at position 2 of MeSA was removed to generate the substrate. The resulting systems contained around 5400 atoms, including ~600 water molecules.

Stochastic Boundary Molecular Dynamics (MD) and Potential Mean Force (PMF) Free Energy Simulations

The stochastic boundary molecular dynamics method⁴¹ was used with the oxygen atom (O_γ) of Ser-81 as the reference center. The reaction region was a sphere with a radius r of 20 Å, and the buffer region extended over the r range of 20–22 Å. All bonds involving hydrogen atoms except those involved in proton transfers in the systems were constrained by the SHAKE algorithm.⁴² The initial structures for the entire stochastic boundary systems were optimized using the steepest descent (SD) and adopted-basis Newton–Raphson (ABNR) methods. The systems were gradually heated from 50.0 to 298.15 K in 100 ps. A 1 fs time step was used for integration of the equation of motion; 500 ps QM/MM MD simulations were conducted for each of the reactant complexes.

The umbrella sampling method⁴³ implemented in CHARMM along with the weighted histogram analysis method (WHAM) was then applied to determine the change in free energy (potential of mean force) as a function of the reaction coordinate (with setting num_MC_trials = 10 and randSeed = 3024 for Monte Carlo bootstrap error analysis; see Figure S1 of the Supporting Information for the results with error bars).⁴⁴ The reaction coordinate (RC) was defined as a linear combination of $r(C\cdots O)$ and $r(C\cdots O_\gamma)$ [$RC = r(C\cdots O) - r(C\cdots O_\gamma)$], as shown in Figure 2. The determination of multidimensional free energy maps would be too time-consuming. Several previous ab initio studies^{45,46} of the catalytic triad systems indicated that the one-dimensional free energy simulations with the selection of a suitable reaction coordinate reflecting the key bond-breaking and bond-making events should be able to capture the key energetic properties for the reaction (e.g., the free energy barrier). For each acylation process, more than 40 windows were used, and for each window, 100 ps simulations were performed with a 50 ps equilibration. The force constants of the harmonic biasing potentials used in the PMF simulations were 50–500 kcal mol⁻¹ Å⁻². The important distances and bond lengths for the average structures of the key states are listed in Table 1.

Table 1. Bond Lengths of Reaction Coordinates

substrate	acylation process	RC ^a	C–O	O _γ –C
MeSA	RS	-1.30 ± 0.05	1.37 ± 0.03	2.67 ± 0.06
	TS1	-0.30 ± 0.06	1.78 ± 0.06	1.48 ± 0.03
	TI	-0.10 ± 0.06	1.63 ± 0.06	1.53 ± 0.04
	TS2	0.40 ± 0.04	1.86 ± 0.03	1.46 ± 0.05
	RS	-1.10 ± 0.05	1.39 ± 0.03	2.48 ± 0.06
MeBA	TS	0.10 ± 0.05	1.67 ± 0.05	1.57 ± 0.04

^aThe reaction coordinate (RC) is defined as the difference between the C–O and O_γ–C distances. The average C–O and O_γ–C distances are given for the RSs, TI, and TSs of the acylation reactions of MeSA and MeBA in tobacco SABP2 obtained from SCC-DFTB/MM free energy simulations (all in angstroms).

Benchmark Calculations. Benchmark calculations with high-level QM/MM calculations have been used by several previous SCC-DFTBPR studies^{47,48} to prove the applicability of SCC-DFTBPR/MM on different enzyme-catalyzed reactions. To the best of our knowledge, this is the first time SCC-DFTB has been applied to study the reaction involving MeSA

(MeBA) with the classic catalytic triad (Ser, His, and Asp). Therefore, benchmark calculations were conducted on the basis of our enzyme complex models to estimate the errors of the SCC-DFTB method in the simulations of the bond-breaking and -making process. First, we compared the optimized structures of the reactant complexes obtained using the B3LYP^{49–51}/MM and SCC-DFTB/MM methods. The QM(B3LYP/6-31G-(d,p))/MM calculations were performed for the acylation processes in SABP2 using the GAMESS-US method⁵² implemented in CHARMM.^{31,32} The basis set [6-31G(d,p)] used here has been successfully used previously in the ab initio QM/MM simulations of acetylcholinesterase.^{53,54}

In addition to comparison of the reactant complex structures, we made similar comparisons on the structures near the transition states as well as the tetrahedral intermediate on the potential energy surfaces. The adiabatic mapping calculations were conducted on the basis of the following protocol. The reaction coordinate is the same as that used in the PMF calculations. A harmonic constraint with a force constant of 2000 kcal mol⁻¹ Å⁻² was added to the RC to guide the SABP2 acylation reaction. The RC value was increased stepwise from the reactant complex to the product complex, with a step size of 0.2 Å. An adopted basis Newton–Raphson (ABNR) minimization was conducted under the constraint. The RC value was then decreased from the product complex to the reactant complex. Forward and backward progress was repeated many times to obtain a smooth and more reliable potential energy surface (PES) profile along the reaction path.

B3LYP/MM Correction of the SCC-DFTB/MM PMF Barrier. Table 2 shows the energetic data from our benchmark calculations. The reaction barriers for the SABP2 acylation reactions with MeSA and MeBA tend to be underestimated by SCC-DFTB/MM compared with B3LYP/MM. Nevertheless, the underestimates of the energies are rather systematic for the different states. A correction for the free energy barrier obtained from the SCC-DFTB results seems to be necessary.^{47,48} The correction used in this work, to be added to the PMF free energy barrier, is the difference in the potential energy barriers from the adiabatic mapping calculations based on the SCC-DFTB/MM and B3LYP/MM methods.

Kinetic Data. The V_{max} values for PtSABP2-1 and PtSABP2-2 using MeSA as a substrate have been experimentally determined in our previous study;²⁵ these values were used to calculate the k_{cat} in each case with the MeSA substrate. The V_{max} values of PtSABP2-1 and PtSABP2-2 using MeBA as a substrate were experimentally determined in this work using the same protocol that was used to determine the V_{max} of PtSABP2-1 (PtSABP2-2) with MeSA.²⁵ PtSABP2-1 and PtSABP2-2 recombinant proteins expressed in *Escherichia coli* were purified and then used in a two-step radiochemical esterase assay to determine the V_{max} values. The obtained V_{max} values were used to calculate the k_{cat} values of PtSABP2-1 and PtSABP2-2 using MeBA as a substrate. The activation barriers for MeSA and MeBA were then obtained on the basis of transition state theory and are listed in Table 2.

RESULTS AND DISCUSSION

As mentioned earlier, the SABP2-catalyzed reaction consists of two steps, acylation and deacylation. The B3LYP/MM potential energy functions of the both acylation and deacylation have been determined for MeSA and MeBA, and the barriers from the potential energy functions suggest that the acylation step is the rate-limiting step in each case (see below).

Table 2. Acylation Free Energy Barriers of SABP2 (kilocalories per mole)

	PtSABP2-1 ^a	PtSABP2-2 ^a	TS1 ^b	TI ^b	TS2 ^b	B3LYP correction ^c
MeSA	18.7	18.4	7.8 (10.6/4.1)	7.1 (10.3/3.9)	9.5 (17.7/12.2)	14.9
	PtSABP2-1 ^a	PtSABP2-2 ^a		TS		B3LYP correction ^c
MeBA	20.4		19.4		11.4 (19.5/14.9)	16.1

^aActivation barriers calculated from transition state theory at 298.15 K based on k_{cat} values. ^bValues without parentheses are from SCC-DFTB/MM PMF simulations. Values in parentheses before and after the slash are from the adiabatic mapping calculations with B3LYP/6-31G(d,p)/MM and SCC-DFTB/MM methods, respectively. ^cThe reaction barriers for the SABP2 acylation reactions with MeSA and MeBA tend to be underestimated by SCC-DFTB/MM compared to those estimated by B3LYP/MM. A correction term for the free energy barrier seems to be necessary. The estimated barrier given here (the last column) was obtained on the basis of the PMF result plus a correction term, which is the difference between the rate-limiting energy barriers (i.e., TS2 for MeSA and TS for MeBA) obtained from the B3LYP/6-31G(d,p)/MM and SCC-DFTB/MM adiabatic mapping calculations. For instance, for MeSA, the correction term is 17.7 kcal/mol – 12.2 kcal/mol = 5.5 kcal/mol, and this was added to 9.5 kcal/mol to obtain the B3LYP-corrected barrier of ~14.9 kcal/mol. The relative energies of the product from the adiabatic mapping calculations are 1.0 kcal/mol (SCC-DFTB) and 4.3 kcal/mol (B3LYP) for the MeSA complex and –2.9 kcal/mol (SCC-DFTB) and –0.2 kcal/mol (B3LYP) for the MeBA complex.

The active site structure of SABP2 complexed with the product SA is plotted in Figure 2 on the basis of the X-ray structure of the SABP2–SA complex.²¹ The catalytic triad (Ser-81, His-238, and Asp-210) is clearly present at the active site. Although there is a hydrogen bond between His-248 and Asp-210, the hydroxyl group of Ser-81 does not form a hydrogen bond with His-238 in the X-ray structure. To perform the nucleophilic attack by Ser-81 on the carbon atom (C) of the substrates, the hydrogen bonding network of the catalytic triad was generated by changing the torsion angle of the side chain of Ser-81; a similar approach has been used in generating a computer model in a previous investigation.²¹ As a result, the residues of the catalytic triad are well-aligned for the nucleophilic attack by Ser-81 on the carbon atom (C) of MeSA, as required for acylation. In the active site of the crystal structure, the oxyanion hole is formed by two hydrogen bonds from SA and Ala-13. It is of interest to note that the amide group of Leu-82 forms a rather weak interaction with the carbonyl group (O) of the substrate with a distance of 3.55 Å. This construction of the oxyanion hole indicates that the two hydrogen bonds (O···O, 2.64 Å; N···O, 2.79 Å) involving SA and Ala-13 may be considerably important for oxyanion hole stabilization and that the weak hydrogen bond from the amide group of Leu-82 (N···O, 3.55 Å) may be enhanced as a result of the development of negative charge during the acylation process.

Acylation Reaction Involving MeSA. MeSA is believed to be the natural substrate of SABP2. The active site structures of SABP2 complexed with MeSA obtained from the B3LYP/MM and SCC-DFTB/MM geometry optimizations are shown in Figure 3a; the initial structures for the optimizations were obtained from different snapshots of the SCC-DFTB/MM molecular dynamics simulations. The optimized structure of the reactant complex from SCC-DFTB/MM shows generally good agreement with that obtained from B3LYP/MM. The hydrogen bonding networks of the catalytic triad are aligned very well via both QM/MM methods. The specific three-pronged oxyanion hole, consisting of two relatively strong hydrogen bonds and a weak one (see above), also agrees well with the crystal structure. Although the geometry optimizations for the reactant state were started from two different snapshots of the SCC-DFTB/MM MD simulations for the two different QM/MM methods, most of the distances obtained from the two QM/MM methods are rather similar. However, there are still some relatively large differences (>0.25 Å) from the two different QM/MM methods. It is of interest to note from Figure 3d that the proton has been transferred away from the side chain of His238, and this is different from the corresponding

result from the PMF simulations (see Figure 4f). At this point, the SCC-DFTB/MM and B3LYP/MM calculations show rather similar results, which is the most important factor for the benchmark calculations. The comparison indicates that overall the SCC-DFTB/MM^{55,56} Hamiltonian is able to provide a reliable description for the structural features of SABP2 complexed with MeSA.

The SCC-DFTB/MM and B3LYP/MM results show the similar trends from the adiabatic mapping calculations as shown in Figure 3a–d. For example, the hydrogen bond from Leu-82 to the substrate is enhanced with developing negative charge on the oxygen upon going from RS to TI. The shapes of potential energy surfaces for the two QM/MM methods also agree well with each other for the two energy ridges (TSs) and a basin (TI) as shown in Table 2; e.g., the free energies at TSs and TI for MeSA are increased systematically by approximately 5.5–6.5 kcal/mol upon going from SCC-DFTB/MM to B3LYP/MM. For the second TS with the highest barrier, the energy barrier was calculated to be ~5.5 kcal/mol lower from SCC-DFTB/MM than that from B3LYP/MM (i.e., 12.2 vs 17.7 kcal/mol). This underestimation by SCC-DFTB/MM in calculating the energy barrier compared to that from high-level QM/MM calculation is consistent with a previous SCC-DFTB study.⁴⁸ In the case presented here, it might be due to an over-stabilization of the transition state or an underestimate of the stability of the reactant by SCC-DFTB, leading to a relatively low barrier. It is of interest to note that the stability of the products seems to be overestimated by SCC-DFTB (Table 2). Although SCC-DFTB still has room for improvement, it seems to be an efficient and reasonably reliable method for determining the relative barriers^{47,48,57} in computer simulations of the acylation reaction of MeSA and MeBA in SABP2. The potential energy functions for the deacylation step were also obtained; e.g., the energy barrier was calculated to be 15.4 kcal/mol from the QM(B3LYP/6-31G(d,p))/MM method for MeSA (compared to 17.7 kcal/mol for acylation). The results suggest that the acylation process is the rate-limiting step.

The free energy profile along the reaction coordinate of the acylation reaction for MeSA obtained from the SCC-DFTB/MM PMF simulations is shown in Figure 4a; the changes in the average distances for $r(\text{C} \cdots \text{O}_y)$ and $r(\text{C} \cdots \text{O})$ are given in Figure 4b. The free energy profile shows that a stable tetrahedral intermediate (TI) (the structure is given in Figure 4e) and two TSs exist during the acylation step. The highest free energy barrier is located at the second TS (see above) with a reaction coordinate of ~0.4 Å. This barrier (9.5 kcal/mol) is significantly lower than the value from the experimental estimate based on k_{cat} (see Table 2). However, this is

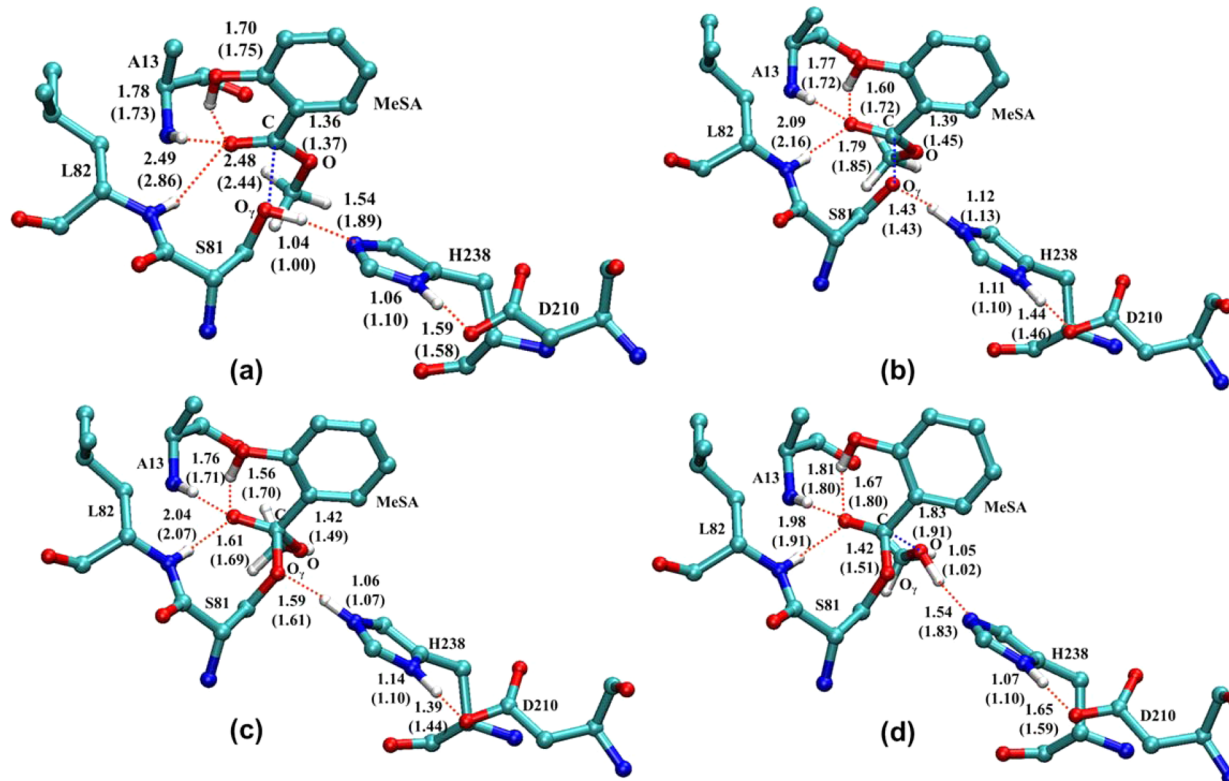


Figure 3. Results from the benchmark calculations for SABP2 complexed with MeSA. Numbers within parentheses are obtained from the SCC-DFTB/MM geometry optimization with dispersion correction; those without parentheses are obtained from the B3LYP/6-31G(d,p)/MM geometry optimization. Most hydrogen atoms have been omitted for the sake of clarity. (a) Reactant state obtained via adiabatic mapping. (b) Structure near transition state 1 obtained via adiabatic mapping. (c) Tetrahedral intermediate obtained via adiabatic mapping. (d) Structure near transition state 2. All distances are in angstroms.

not surprising because the benchmark calculations based on adiabatic mapping (see *discussions* above) found that SCC-DFTB/MM systematically underestimates the potential energies compared to B3LYP/MM. If a correction of 5.5 kcal/mol (the difference between the SCC-DFTB/MM and B3LYP/MM barriers from the adiabatic mapping) is used, the estimated barrier for acylation from the simulations would be \sim 15 kcal/mol. It should be pointed out that the key purpose of this study is to compare the relative catalytic efficiencies of SABP2 on MeSA and MeBA and examine the role of SAC from MeSA. Much of the error in the computational methods is expected to be canceled out because of the fact that they are used for the same reaction process with very similar structural features of the substrates.

Figure 4b shows that the distances and bond lengths of $r(C\cdots O)$ and $r(C-O_1)$ change smoothly and intersect at an RC around 0 Å; some average distances and bond lengths in RS, TSs, and TI are summarized in Table 1. Panels c–f of Figure 4 show that the average structures along the reaction path share properties similar to those in the optimized structures obtained earlier (Figure 3a–d). As expected, the role of the catalytic triad in the acylation process seems to be the same as in the case of classic serine proteases.^{45,58} For instance, the carboxylate of Asp-208 works with the incipient imidazolium cation to stabilize the TS and the TI through electrostatic interactions.^{58,59}

We also examined the changes in the hydrogen-bond distances for the hydrogen bonds involved in the three-pronged oxyanion hole interactions (Ala-13, Leu-82, and the MeSA hydroxyl group). In RS (Figure 4a), the two hydrogen bonds are formed between the MeSA carbonyl group (O1) and the

amide group of Ala-13 and between the MeSA carbonyl and hydroxyl groups, with N \cdots O and O \cdots O distances of 1.90 and 1.80 Å, respectively. It is of interest to note that the amide group of Leu-82 forms a rather weak interaction with O1 of the substrate with a distance of 2.96 Å in the RS. Thus, the enzyme seems to contain a less effective oxyanion hole from its functional groups for the stabilization of the tetrahedral intermediates (TIs) during the catalysis. Interestingly, the 2-OH group of MeSA forms a strong hydrogen bond with O1 with a hydrogen-bond distance of 1.67 Å. Moreover, this hydrogen bond seems to strengthen significantly as the reaction proceeds from the reactant complex to the tetrahedral intermediate (see Figure 4c–f) based on the PMF simulations. Thus, the 2-OH group from the MeSA substrate may help to generate a more effective oxyanion hole for lowering the activation barrier through SAC and contribute to the relatively high specificity of SABP2 toward MeSA.

Acylation Reaction Involving MeBA. To test the hypothesis concerning the importance of SAC in substrate discrimination, the acylation reaction involving methyl benzoate (MeBA) was also studied. MeBA is presumably a substrate of SABP2, as well, and has a structure very similar to that of MeSA except that it lacks the 2-OH hydroxyl group.

Similar to the case involving MeSA (see above), the results obtained from the SCC-DFTB/MM energy minimization for the SABP2–MeBA complex are quite similar to those from the B3LYP/MM calculations (Figure 5a,b). However, unlike the case involving MeSA, there is no stable intermediate obtained from the calculations (see below). In the optimized structure of RS (Figure 5a), the similar patterns of the hydrogen bonding

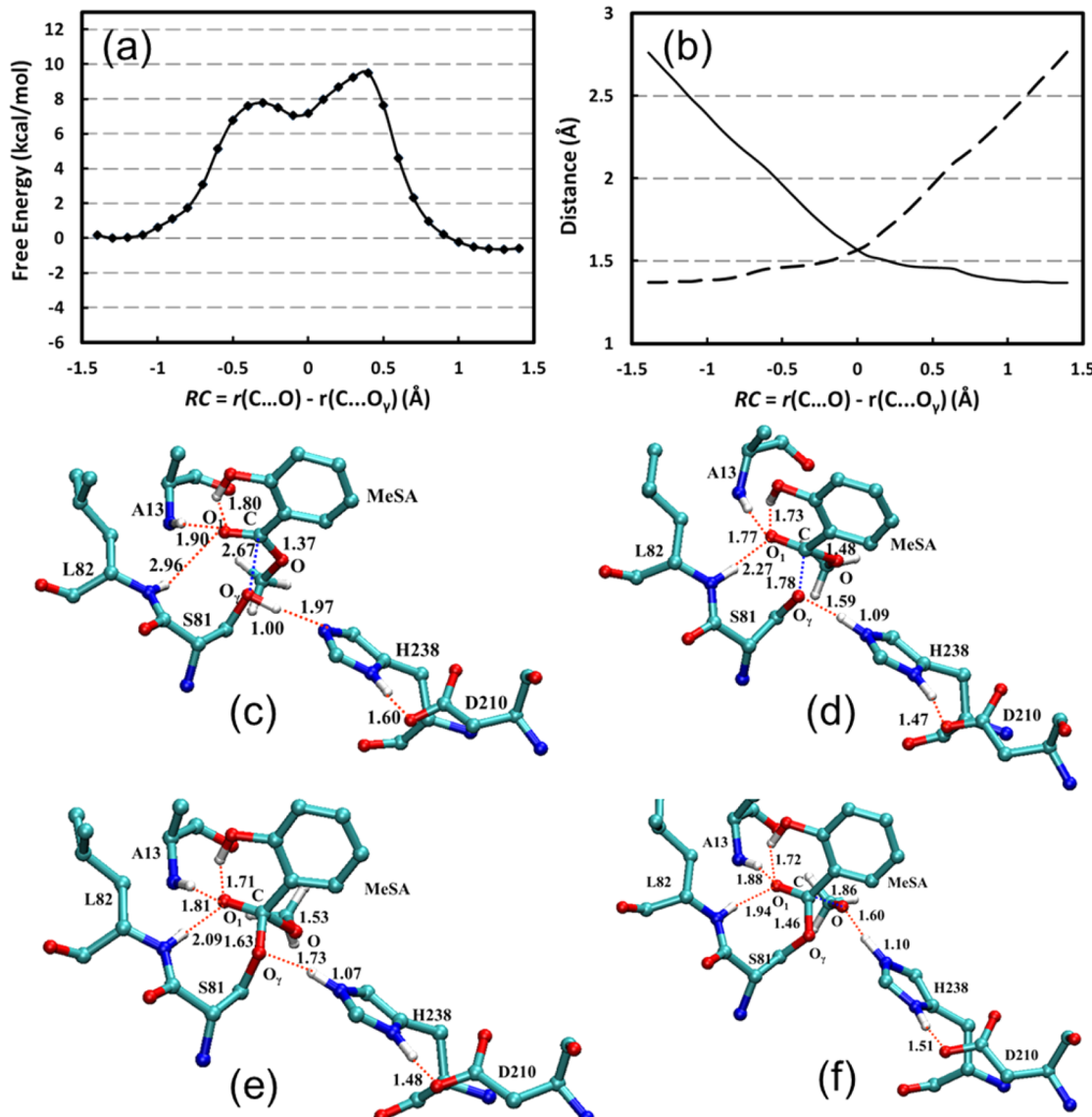


Figure 4. PMF results for SABP2 complexed with MeSA with SCC-DFTB/MM. (a) The free energy profile along the reaction coordinate. See Figure S1A for the same profile with error bars. (b) Changes in the average distances along the reaction coordinate: (—) $r(C\cdots O_y)$ and (---) $r(C\cdots O)$. (c) Average structure of the reactant state. (d) Average structure near the first transition state. (e) Average structure of the tetrahedral intermediate. (f) Average structure near the second transition state. Most hydrogen atoms have been omitted for the sake of clarity. Distances are in angstroms, and free energies are in kilocalories per mole.

networks are obtained from the calculations using the two different methods. It can be seen from Figure 5a that without the OH group on the substrate, a two-pronged oxyanion hole is formed in the SABP2–MeBA complex instead of the three-pronged one as observed in the SABP2–MeSA complex. The amide group of Leu-82 is closer to O1 of the MeBA carbonyl group (approximately 2.3–2.4 Å) compared to that in the MeSA complex. Nevertheless, the corresponding hydrogen bond still seems to be considerably weaker than the hydrogen bond involving Ala-13 with a hydrogen-bond distance of 1.7–1.8 Å. Similar to the case involving MeSA, the SCC-DFTB/MM method underestimates the energy barrier by ~4.6 kcal/mol based on the adiabatic mapping calculations (Table 2). The structures near the TS from the two different QM/MM methods are quite similar (Figure 5b). Moreover, the proton has been transferred from the side chain of His-238; this phenomenon has been observed in the MeSA benchmark calculations and discussed earlier.

The free energy (PMF) profile obtained with the SCC-DFTB/MM method is given in Figure 6. Figure 6 shows that, as expected, there is only one TS located at an RC of ~0.1 Å. The C–O and C– O_y distances are plotted as a function of RC in Figure 6b. Similar to the case involving MeSA, $r(C\cdots O)$ and $r(C\cdots O_y)$ change smoothly and intersect at an RC of ~0 Å. The free energy barrier is calculated to be 11.4 kcal/mol, which is ~2 kcal/mol higher than the barrier in the case involving MeSA. As is shown in Table 2, this barrier is likely underestimated by ~4.6 kcal/mol because of the systematic error of SCC-DFTB. After the barrier correction based on comparison of the results from the adiabatic mapping calculations with the different QM/MM methods (see above), the estimate for the free energy barrier is ~16.1 kcal/mol (Table 2), which is 1.2 kcal/mol higher than the estimate for the free energy barrier of MeSA with a similar correction.

Comparison with Experiments. To confirm the theoretical prediction concerning the involvement of the hydroxyl

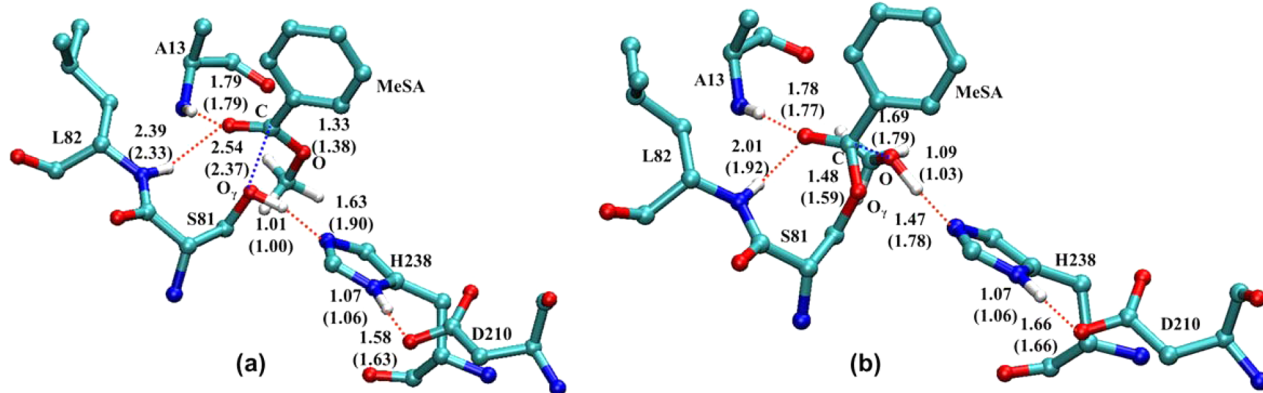


Figure 5. Results from the benchmark calculations for SABP2 complexed with MeBA. Numbers within parentheses are obtained from the SCC-DFTB/MM geometry optimization with dispersion correction; those without parentheses are obtained from the B3LYP/6-31G(d,p)/MM geometry optimization. (a) Reactant state obtained via adiabatic mapping. (b) Structure near the transition state (TS). All distances are in angstroms.

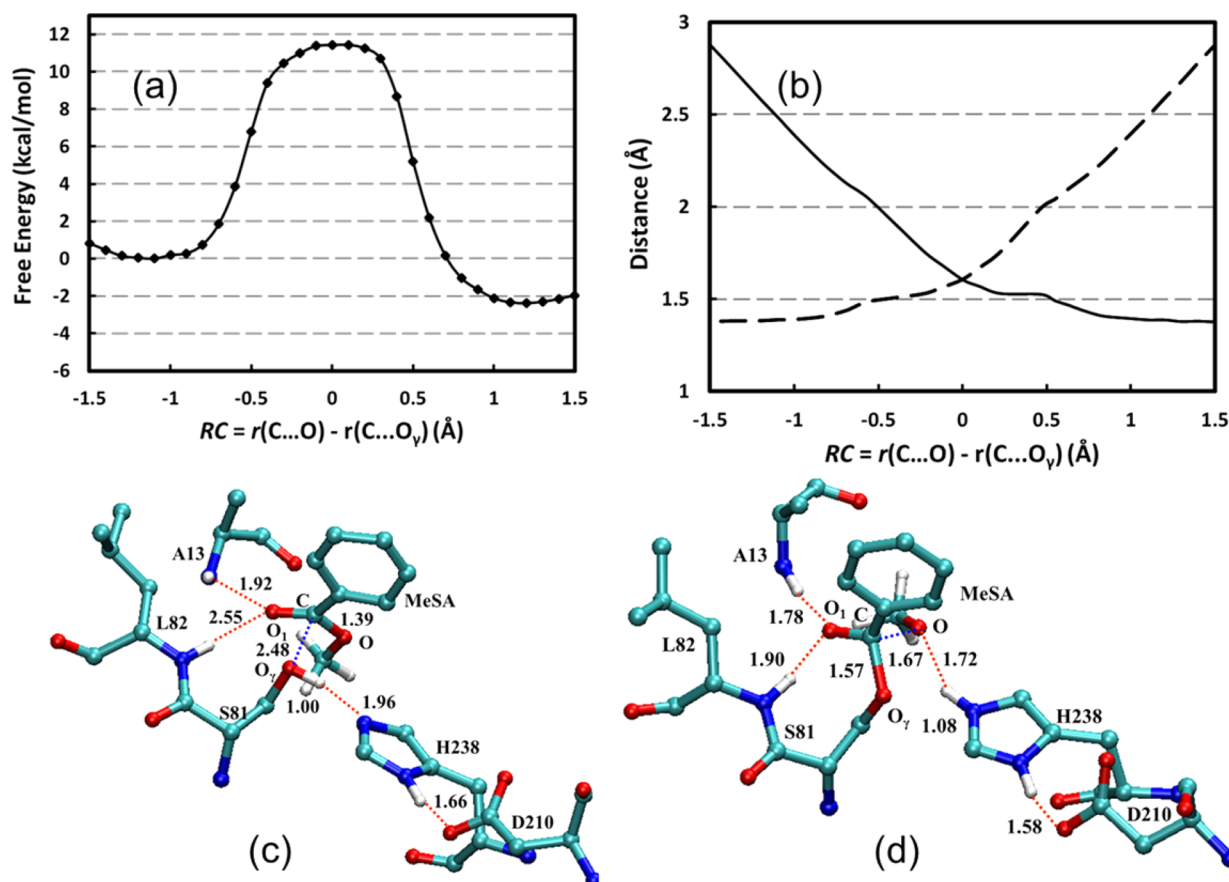


Figure 6. PMF results for SABP2 complexed with MeBA with SCC-DFTB/MM. (a) Free energy profile along the reaction coordinate. See Figure S1B for error bars. (b) Changes in the average distances along the reaction coordinate: (—) $r(C\cdots O_y)$ and (---) $r(C\cdots O)$. (c) Reactant state. (d) Transition state. Distances are in angstroms, and energies are in kilocalories per mole.

group of MeSA in SAC and substrate discrimination, we measured the esterase activities of PtSABP2-1 and PtSABP2-2 toward MeBA and compared them with the corresponding activities of these enzymes toward MeSA²⁵ (Table 2). PtSABP2-1 and PtSABP2-2 are 98% identical to each other and have sequences >77% identical to that of tobacco SABP2.²¹ Their activity profiles for different substrates were found to be rather similar to that of tobacco SABP2.²¹ For instance, it was observed²¹ that for tobacco SABP2 the esterase activity with MeIAA and MeJA was less than 15% of that with MeSA at substrate concentrations of 10 and 100 μ M,

and no MeJA esterase activity was observed at 10 μ M substrate concentration. For PtSABP2-1 and PtSABP2-2, we showed previously²⁵ that at 10 and 100 μ M substrate concentration both enzymes had no or very low activity with MeIAA and MeJA. Moreover, the esterase activities of PtSABP2-1 and PtSABP2-2 with MeJA are only 9 and 14% of their corresponding activities with MeSA, respectively, at 1 mM substrate. These results indicate that the three enzymes are highly specific for MeSA among the substrates tested at both physiologically relevant (10 μ M) and irrelevant (1 mM) concentrations.

Consistent with the results of the theoretical calculations, for PtSABP2-1 the activation barriers were found to be 18.7 and 20.4 kcal/mol for MeSA and MeBA, respectively, based on their k_{cat} values (0.120 s^{-1} for MeSA and 0.007 s^{-1} for MeBA) from this and the earlier work²⁵ as well as transition state theory. Correspondingly, the K_M (k_{cat}/K_M) values were found to be $68.2\text{ }\mu\text{M}$ ($1.76 \times 10^3\text{ s}^{-1}\text{ M}^{-1}$) and $39.6\text{ }\mu\text{M}$ ($1.77 \times 10^2\text{ s}^{-1}\text{ M}^{-1}$) for MeSA and MeBA, respectively. Similar to the case for PtSABP2-1, the activation barriers for PtSABP2-2 based on the k_{cat} values for MeSA (0.187 s^{-1}) and MeBA (0.038 s^{-1}) were estimated to be 18.4 and 19.4 kcal/mol, respectively; the K_M (k_{cat}/K_M) values were found to be $24.6\text{ }\mu\text{M}$ ($7.6 \times 10^3\text{ s}^{-1}\text{ M}^{-1}$) and $42.1\text{ }\mu\text{M}$ ($9 \times 10^2\text{ s}^{-1}\text{ M}^{-1}$) for MeSA and MeBA, respectively. Thus, the difference in the experimental activation barriers for MeSA and MeBA in both PtSABP2-1 and PtSABP2-2 is $\sim 1.0\text{--}1.7$ kcal/mol. Moreover, the k_{cat}/K_M values for MeSA in these enzymes are approximately 8.5–10 times higher than the corresponding values for MeBA. The relatively high activities involving MeSA may be attributed to the existence of the interaction involving the 2-OH group in MeSA, as we discussed earlier. This hydrogen bond can presumably increase the effectiveness of the oxyanion–hole interaction and provide additional stabilization for TS (TI). Consistent with this suggestion, several previous studies of the oxyanion hole showed that disturbing the electrostatic interaction of a hydrogen bond or destroying the oxyanion hole may cause an increase in the barrier of 1.5–3.0 kcal/mol for thrombin and trypsin⁶⁰ and abrogation of the catalytic activities of subtilisin⁶¹ and serine-carboxyl peptidase.^{62,63}

CONCLUSIONS

Many enzymes have been found to possess a remarkable ability to discriminate between their natural substrates and closely related molecules.^{64,65} However, our understanding of this ability of enzymes is still lacking. Our results here show that SABP2 may contain a less perfect oxyanion hole, with the additional contribution coming from the natural substrate MeSA. For other compounds and substrates without such a well-positioned functional group, the catalysis would be less efficient and the discrimination between MeSA and these compounds would then be achieved. Our results therefore support the suggestion that some naturally occurring enzymes might have already used SAC as one of its important strategies for substrate discrimination. The experimental data for PtSABP2-1 and PtSABP2-2 seem to support our theoretical prediction that the participation of the 2-OH group for the catalysis may contribute, at least in part, to the relatively strong esterase activity of these enzymes toward MeSA. It would be of considerable interest to examine whether other naturally occurring enzymes would use SAC for substrate discrimination, as well.

ASSOCIATED CONTENT

Supporting Information

The Supporting Information is available free of charge on the ACS Publications website at DOI: [10.1021/acs.biochem.5b00638](https://doi.org/10.1021/acs.biochem.5b00638).

The PMFs of Figures 4 and 6 contain error bars (Figure S1) ([PDF](#))

AUTHOR INFORMATION

Corresponding Author

*Department of Biochemistry and Cellular and Molecular Biology, University of Tennessee, Knoxville, TN 37996, and UT/ORNL Center for Molecular Biophysics, Oak Ridge National

Laboratory, Oak Ridge, TN 37830. E-mail: hguo1@utk.edu.
Fax: +1 (865) 974-6306.

Funding

This work was supported in part by Grant 0817940 from the National Science Foundation (H.G.) and by the Department of Energy Office of Biological and Environmental Research—Genome to Life Program through the BioEnergy Science Center (BESC) (to F.C.). Oak Ridge National Laboratory is managed by UT-Battelle, LLC, for the U.S. Department of Energy (under Contract DE-AC05-00OR22725). This work used the Extreme Science and Engineering Discovery Environment (XSEDE), which is supported by National Science Foundation Grant ACI-1053575.

Notes

The authors declare no competing financial interest.

REFERENCES

- (1) Hult, K., and Berglund, P. (2007) Enzyme promiscuity: mechanism and applications. *Trends Biotechnol.* 25, 231–238.
- (2) Nath, A., and Atkins, W. M. (2008) A Quantitative Index of Substrate Promiscuity. *Biochemistry* 47, 157–166.
- (3) Huang, F.-C., Horváth, G., Molnár, P., Turcsi, E., Deli, J., Schrader, J., Sandmann, G., Schmidt, H., and Schwab, W. (2009) Substrate promiscuity of RdCCD1, a carotenoid cleavage oxygenase from *Rosa damascena*. *Phytochemistry* 70, 457–464.
- (4) Faridmoayer, A., Fentabil, M. A., Haurat, M. F., Yi, W., Woodward, R., Wang, P. G., and Feldman, M. F. (2008) Extreme Substrate Promiscuity of the Neisseria Oligosaccharyl Transferase Involved in Protein O-Glycosylation. *J. Biol. Chem.* 283, 34596–34604.
- (5) Theodossis, A., Walden, H., Westwick, E. J., Connaris, H., Lamble, H. J., Hough, D. W., Danson, M. J., and Taylor, G. L. (2004) The Structural Basis for Substrate Promiscuity in 2-Keto-3-deoxygluconate Aldolase from the Entner-Doudoroff Pathway in *Sulfolobus solfataricus*. *J. Biol. Chem.* 279, 43886–43892.
- (6) Cohen-Rosenzweig, C., Guan, Z., Shaanan, B., and Eichler, J. (2014) Substrate Promiscuity: AglB, the Archaeal Oligosaccharyl-transferase, Can Process a Variety of Lipid-Linked Glycans. *Appl. Environ. Microbiol.* 80, 486–496.
- (7) Aharoni, A., Gaidukov, L., Khersonsky, O., Gould, S. M., Roodveldt, C., and Tawfik, D. S. (2005) The ‘evolvability’ of promiscuous protein functions. *Nat. Genet.* 37, 73–76.
- (8) Khersonsky, O., Roodveldt, C., and Tawfik, D. S. (2006) Enzyme promiscuity: evolutionary and mechanistic aspects. *Curr. Opin. Chem. Biol.* 10, 498–508.
- (9) Babtie, A., Tokuriki, N., and Hollfelder, F. (2010) What makes an enzyme promiscuous? *Curr. Opin. Chem. Biol.* 14, 200–207.
- (10) Khersonsky, O., and Tawfik, D. S. (2010) Enzyme Promiscuity: A Mechanistic and Evolutionary Perspective. *Annu. Rev. Biochem.* 79, 471–505.
- (11) Gatti-Lafranconi, P., and Hollfelder, F. (2013) Flexibility and Reactivity in Promiscuous Enzymes. *ChemBioChem* 14, 285–292.
- (12) Kopycki, J. G., Rauh, D., Chumanovich, A. A., Neumann, P., Vogt, T., and Stubbs, M. T. (2008) Biochemical and Structural Analysis of Substrate Promiscuity in Plant Mg²⁺-Dependent O-Methyltransferases. *J. Mol. Biol.* 378, 154–164.
- (13) Sabini, E., Hazra, S., Ort, S., Konrad, M., and Lavie, A. (2008) Structural Basis for Substrate Promiscuity of dCK. *J. Mol. Biol.* 378, 607–621.
- (14) Carter, P., and Wells, J. A. (1987) Engineering enzyme specificity by substrate-assisted catalysis. *Science* 237, 394–399.
- (15) Carter, P., Nilsson, B., Burnier, J. P., Burdick, D., and Wells, J. A. (1989) Engineering subtilisin bpn' for site-specific proteolysis. *Proteins: Struct., Funct., Genet.* 6, 240–248.
- (16) Xu, Q., Guo, H., Wlodawer, A., and Guo, H. (2006) The importance of dynamics in substrate-assisted catalysis and specificity. *J. Am. Chem. Soc.* 128, 5994–5995.

- (17) Bornscheuer, U. T., and Kazlauskas, R. J. (2004) Catalytic Promiscuity in Biocatalysis: Using Old Enzymes to Form New Bonds and Follow New Pathways. *Angew. Chem., Int. Ed.* 43, 6032–6040.
- (18) Lairson, L. L., Watts, A. G., Wakarchuk, W. W., and Withers, S. G. (2006) Using substrate engineering to harness enzymatic promiscuity and expand biological catalysis. *Nat. Chem. Biol.* 2, 724–728.
- (19) Lewinson, O., Adler, J., Sigal, N., and Bibi, E. (2006) Promiscuity in multidrug recognition and transport: the bacterial MFS Mdr transporters. *Mol. Microbiol.* 61, 277–284.
- (20) Fernández, A., Tawfik, D. S., Berkhouit, B., Sanders, R., Kloczkowski, A., Sen, T., Jernigan, B., Tawfik, D. S., Berkhouit, B., Sanders, R. W., Kloczkowski, A., Sen, T. Z., and Jernigan, R. L. (2005) Protein Promiscuity: Drug Resistance and Native Functions—HIV-1 Case. *J. Biomol. Struct. Dyn.* 22, 615–624.
- (21) Forouhar, F., Yang, Y., Kumar, D., Chen, Y., Fridman, E., Park, S. W., Chiang, Y., Acton, T. B., Montelione, G. T., Pichersky, E., Klessig, D. F., and Tong, L. (2005) Structural and biochemical studies identify tobacco SABP2 as a methyl salicylate esterase and implicate it in plant innate immunity. *Proc. Natl. Acad. Sci. U. S. A.* 102, 1773–1778.
- (22) Kumar, D., Gustafsson, C., and Klessig, D. F. (2006) Validation of RNAi silencing specificity using synthetic genes: salicylic acid-binding protein 2 is required for innate immunity in plants. *Plant J.* 45, 863–868.
- (23) Kumar, D., and Klessig, D. F. (2003) High-affinity salicylic acid-binding protein 2 is required for plant innate immunity and has salicylic acid-stimulated lipase activity. *Proc. Natl. Acad. Sci. U. S. A.* 100, 16101–16106.
- (24) Kumar, D., Park, S., Forouhar, F., Yang, Y., Vlot, A., Fridman, E., Chiang, Y., Acton, T., Shulaev, V., Montelione, G., Pichersky, E., Tong, L., and Klessig, D. (2005) Identification of SA-binding protein 2 (SABP2) as a critical component of plant innate immunity. *Phytopathology* 95, S55–S55.
- (25) Zhao, N., Guan, J., Forouhar, F., Tschaplinski, T. J., Cheng, Z. M., Tong, L., and Chen, F. (2009) Two poplar methyl salicylate esterases display comparable biochemical properties but divergent expression patterns. *Phytochemistry* 70, 32–39.
- (26) Yao, J., Xu, Q., Chen, F., and Guo, H. (2011) QM/MM Free Energy Simulations of Salicylic Acid Methyltransferase: Effects of Stabilization of TS-like Structures on Substrate Specificity. *J. Phys. Chem. B* 115, 389–396.
- (27) Padhi, S. K., Fujii, R., Legatt, G. A., Fossum, S. L., Berchtold, R., and Kazlauskas, R. J. (2010) Switching from an Esterase to a Hydroxynitrile Lyase Mechanism Requires Only Two Amino Acid Substitutions. *Chem. Biol.* 17, 863–871.
- (28) Tripathi, D., Jiang, Y.-L., and Kumar, D. (2010) SABP2, a methyl salicylate esterase is required for the systemic acquired resistance induced by acibenzolar-S-methyl in plants. *FEBS Lett.* 584, 3458–3463.
- (29) Cui, Q., Elstner, M., Kaxiras, E., Frauenheim, T., and Karplus, M. (2001) A QM/MM Implementation of the Self-Consistent Charge Density Functional Tight Binding (SCC-DFTB) Method. *J. Phys. Chem. B* 105, 569–585.
- (30) Brünger, A. T., and Karplus, M. (1988) Polar hydrogen positions in proteins: Empirical energy placement and neutron diffraction comparison. *Proteins: Struct., Funct., Genet.* 4, 148–156.
- (31) Brooks, B. R., Bruccoleri, R. E., Olafson, B. D., States, D. J., Swaminathan, S., and Karplus, M. (1983) Charmm - a program for macromolecular energy, minimization, and dynamics calculations. *J. Comput. Chem.* 4, 187–217.
- (32) Brooks, B. R., Brooks, C. L., Mackerell, A. D., Nilsson, L., Petrella, R. J., Roux, B., Won, Y., Archontis, G., Bartels, C., Boresch, S., Caflisch, A., Caves, L., Cui, Q., Dinner, A. R., Feig, M., Fischer, S., Gao, J., Hodoscek, M., Im, W., Kuczera, K., Lazaridis, T., Ma, J., Ovchinnikov, V., Paci, E., Pastor, R. W., Post, C. B., Pu, J. Z., Schaefer, M., Tidor, B., Venable, R. M., Woodcock, H. L., Wu, X., Yang, W., York, D. M., and Karplus, M. (2009) CHARMM: The Biomolecular Simulation Program. *J. Comput. Chem.* 30, 1545–1614.
- (33) Molecular Operating Environment (MOE), version 2013.08 (2015) Chemical Computing Group Inc., Montreal.
- (34) Jorgensen, W. L. (1981) quantum and statistical mechanical studies of liquids 0.10. Transferable intermolecular potential functions for water, alcohols, and ethers - application to liquid water. *J. Am. Chem. Soc.* 103, 335–340.
- (35) Neria, E., Fischer, S., and Karplus, M. (1996) Simulation of activation free energies in molecular systems. *J. Chem. Phys.* 105, 1902–1921.
- (36) Field, M. J., Bash, P. A., and Karplus, M. (1990) A combined quantum-mechanical and molecular mechanical potential for molecular-dynamics simulations. *J. Comput. Chem.* 11, 700–733.
- (37) König, P. H., Hoffmann, M., Frauenheim, T., and Cui, Q. (2005) A Critical Evaluation of Different QM/MM Frontier Treatments with SCC-DFTB as the QM Method. *J. Phys. Chem. B* 109, 9082–9095.
- (38) Cui, Q., Elstner, M., Kaxiras, E., Frauenheim, T., and Karplus, M. (2001) A QM/MM implementation of the self-consistent charge density functional tight binding (SCC-DFTB) method. *J. Phys. Chem. B* 105, 569–585.
- (39) Elstner, M., Hobza, P., Frauenheim, T., Suhai, S., and Kaxiras, E. (2001) Hydrogen bonding and stacking interactions of nucleic acid base pairs: A density-functional-theory based treatment. *J. Chem. Phys.* 114, 5149–5155.
- (40) MacKerell, A. D., Bashford, D., Bellott, M., Dunbrack, R. L., Evanseck, J. D., Field, M. J., Fischer, S., Gao, J., Guo, H., Ha, S., Joseph-McCarthy, D., Kuchnir, L., Kuczera, K., Lau, F. T. K., Mattos, C., Michnick, S., Ngo, T., Nguyen, D. T., Prodhom, B., Reiher, W. E., Roux, B., Schlenkrich, M., Smith, J. C., Stote, R., Straub, J., Watanabe, M., Wiorkiewicz-Kuczera, J., Yin, D., and Karplus, M. (1998) All-atom empirical potential for molecular modeling and dynamics studies of proteins. *J. Phys. Chem. B* 102, 3586–3616.
- (41) Brooks, C. L., Brünger, A., and Karplus, M. (1985) Active-site dynamics in protein molecules - a stochastic boundary molecular-dynamics approach. *Biopolymers* 24, 843–865.
- (42) Ryckaert, J. P., Cicotti, G., and Berendsen, H. J. C. (1977) Numerical-integration of cartesian equations of motion of a system with constraints - molecular-dynamics of n-alkanes. *J. Comput. Phys.* 23, 327–341.
- (43) Torrie, G. M., and Valleau, J. P. (1974) Monte-carlo free-energy estimates using non-boltzmann sampling - application to subcritical lennard-jones fluid. *Chem. Phys. Lett.* 28, 578–581.
- (44) Grossfield, A. WHAM: The weighted histogram analysis method, version 2.0.9, University of Rochester Medical Center, Rochester, NY (<http://membrane.urmc.rochester.edu/content/wham>).
- (45) Zhang, Y., Kua, J., and McCammon, J. A. (2002) Role of the Catalytic Triad and Oxylanion Hole in Acetylcholinesterase Catalysis: An ab initio QM/MM Study. *J. Am. Chem. Soc.* 124, 10572–10577.
- (46) Ishida, T., and Kato, S. (2003) Theoretical Perspectives on the Reaction Mechanism of Serine Proteases: The Reaction Free Energy Profiles of the Acylation Process. *J. Am. Chem. Soc.* 125, 12035–12048.
- (47) Hou, G., and Cui, Q. (2012) QM/MM Analysis Suggests That Alkaline Phosphatase (AP) and Nucleotide Pyrophosphatase/Phosphodiesterase Slightly Tighten the Transition State for Phosphate Diester Hydrolysis Relative to Solution: Implication for Catalytic Promiscuity in the AP Superfamily. *J. Am. Chem. Soc.* 134, 229–246.
- (48) Hou, G., and Cui, Q. (2013) Stabilization of Different Types of Transition States in a Single Enzyme Active Site: QM/MM Analysis of Enzymes in the Alkaline Phosphatase Superfamily. *J. Am. Chem. Soc.* 135, 10457–10469.
- (49) Becke, A. D. (1988) Density-functional exchange-energy approximation with correct asymptotic behavior. *Phys. Rev. A: At., Mol., Opt. Phys.* 38, 3098–3100.
- (50) Lee, C., Yang, W., and Parr, R. G. (1988) Development of the Colle-Salvetti correlation-energy formula into a functional of the electron density. *Phys. Rev. B: Condens. Matter Mater. Phys.* 37, 785–789.
- (51) Becke, A. D. (1993) Density-functional thermochemistry. III. The role of exact exchange. *J. Chem. Phys.* 98, 5648–5652.

- (52) Schmidt, M. W., Baldridge, K. K., Boatz, J. A., Elbert, S. T., Gordon, M. S., Jensen, J. H., Koseki, S., Matsunaga, N., Nguyen, K. A., Su, S. J., Windus, T. L., Dupuis, M., and Montgomery, J. A. (1993) General atomic and molecular electronic-structure system. *J. Comput. Chem.* 14, 1347–1363.
- (53) Sirin, G. S., Zhou, Y., Lior-Hoffmann, L., Wang, S., and Zhang, Y. (2012) Aging Mechanism of Soman Inhibited Acetylcholinesterase. *J. Phys. Chem. B* 116, 12199–12207.
- (54) Zhou, Y., Wang, S., and Zhang, Y. (2010) Catalytic Reaction Mechanism of Acetylcholinesterase Determined by Born–Oppenheimer Ab Initio QM/MM Molecular Dynamics Simulations. *J. Phys. Chem. B* 114, 8817–8825.
- (55) Gaus, M., Cui, Q., and Elstner, M. (2011) DFTB3: Extension of the Self-Consistent-Charge Density-Functional Tight-Binding Method (SCC-DFTB). *J. Chem. Theory Comput.* 7, 931–948.
- (56) Yang, Yu, H., York, D., Cui, Q., and Elstner, M. (2007) Extension of the Self-Consistent-Charge Density-Functional Tight-Binding Method: Third-Order Expansion of the Density Functional Theory Total Energy and Introduction of a Modified Effective Coulomb Interaction. *J. Phys. Chem. A* 111, 10861–10873.
- (57) Hou, G., Zhu, X., Elstner, M., and Cui, Q. (2012) A Modified QM/MM Hamiltonian with the Self-Consistent-Charge Density-Functional-Tight-Binding Theory for Highly Charged QM Regions. *J. Chem. Theory Comput.* 8, 4293–4304.
- (58) Blow, D. M. (1976) Structure and mechanism of chymotrypsin. *Acc. Chem. Res.* 9, 145–152.
- (59) Warshel, A., Naray-Szabo, G., Sussman, F., and Hwang, J. K. (1989) How do serine proteases really work? *Biochemistry* 28, 3629–3637.
- (60) Bobofchak, K. M., Pineda, A. O., Mathews, F. S., and Di Cera, E. (2005) Energetic and Structural Consequences of Perturbing Gly-193 in the Oxyanion Hole of Serine Proteases. *J. Biol. Chem.* 280, 25644–25650.
- (61) Bryan, P., Pantoliano, M. W., Quill, S. G., Hsiao, H. Y., and Poulos, T. (1986) Site-directed mutagenesis and the role of the oxyanion hole in subtilisin. *Proc. Natl. Acad. Sci. U. S. A.* 83, 3743–3745.
- (62) Yao, J., Xu, Q., and Guo, H. (2013) QM/MM and free-energy simulations of deacylation reaction catalysed by sedolisin, a serine-carboxyl peptidase. *Mol. Simul.* 39, 206–213.
- (63) Xu, Q., Yao, J., Wlodawer, A., and Guo, H. (2011) Clarification of the Mechanism of Acylation Reaction and Origin of Substrate Specificity of the Serine-Carboxyl Peptidase Sedolisin through QM/MM Free Energy Simulations. *J. Phys. Chem. B* 115, 2470–2476.
- (64) Fersht, A. (1998) *Structure and Mechanism in Protein Science*, W. H. Freeman and Co., New York.
- (65) Hedstrom, L. (2002) Serine protease mechanism and specificity. *Chem. Rev.* 102, 4501–4523.